Green Energy and Fuel Research

Scilight

Article

Current Potentials and Challenges in Designing Co-Electrolysis Systems for CO_2 Conversion

Kuan-Wen Chen †, Ching-Han Lu † and Bor-Yih Yu *

Department of Chemical Engineering, National Taiwan University, Taipei 106319, Taiwan
* Correspondence: boryihyu@ntu.edu.tw
† These authors contributed equally to this work.
Received: 2 June 2026; Revised: 4 August 2026; Accepted: 6 August 2026; Published: 12 August 2026

Abstract: Electrochemical CO_2 reduction (ECO_2RR) provides a promising route for its conversion into fuels and value-added chemicals using renewable electricity. Recent advancements have explored the integration of cathodic ECO_2RR with various anodic organic oxidation reactions (OOR) to enhance economic feasibility and lower operating potentials. However, process-level insights into these integrated systems remain largely unexplored. The numerous potential combinations of ECO_2RR and OOR make it impractical to conduct detailed process designs for every pairing. In this paper, we review existing half-reaction experiments and establish a framework to screen for potential integrations of OOR and ECO_2RR based on reported technical feasibility and economic margins. From our framework, we have identified seven candidate pairing systems, predominantly demonstrating economic margins ranging from \$0.1 to \$0.4 per kg of product. In addition, we highlight the practical challenges encountered in downstream processing, particularly the recovery of ionic products from dilute reaction media. Overall, we conclude that co-electrolysis is economically viable when the added value from the anodic reaction provides sufficient margins to offset downstream separation and purification costs (e.g., pairing methanol and glycolic acid production), or when both half-reactions yield identical products (e.g., formate), which significantly simplifies downstream processing.

Keywords: CCUS; electrochemical reduction; coelectrolysis; organic oxidative reaction; process design

1. Introduction

Carbon dioxide (CO_2) reduction is a vital part of current carbon capture and utilization research. Traditionally, thermal catalysis is used to transform CO_2 into valuable chemicals. Examples include the production of hydrocarbons [1,2], alcohols [3], carbonates [4], carbamates [5], and others. While this method is well established, it usually requires high temperatures and high pressures. In addition, expensive green hydrogen is often assumed in relevant research, leading to economic barriers and practical limitations for regions with limited green electricity. Other emerging methods include photocatalysis and biocatalysis. Photocatalysis uses direct solar energy but currently suffers from low efficiency and poor stability [6]. Multi-carbon product formation remains particularly challenging because efficient charge transfer and C-C coupling are both required [7]. Biocatalysis offers high selectivity for products like biodegradable plastics, but it remains very difficult to scale up due to high costs and low production rates.

Electrochemical CO_2 reduction reaction (ECO_2RR) emerges as a competitive alternative [8]. Operating at room temperature and standard pressure significantly reduces the safety risks and overall energy requirements. Driven by electricity, the process can be easily integrated with renewable energy sources. It offers a modular design and high selectivity for products such as carbon monoxide, methanol, ethanol, and formic acid [9–12]. These compact electrolyzers can be deployed directly near industrial emission sources to facilitate efficient carbon recycling. Electrolyzers are broadly divided into solid and liquid systems based on their operating temperatures. High-temperature solid electrolyzers operate between 600 and 800 °C to efficiently produce carbon monoxide [13]. Meanwhile, low-temperature liquid electrolyzers operate between 25 and 80 °C [14]. With proper catalyst design, these low-temperature systems use water directly as a clean hydrogen source, offering an eco-friendly way to generate the valuable chemicals mentioned earlier [15,16].

Mechanistically, ECO_2RR typically involves gas adsorption, electron transfer, and product desorption. While generating single carbon products (e.g., CO, formic acid) is straightforward, producing multi-carbon chemicals is much more challenging because of the high energy barriers for C-C coupling [17]. Previous research has extensively attempted to address these thermodynamic and kinetic issues through advanced catalyst design and surface engineering [18,19]. However, most of those studies remain at the fundamental level. Metrics such as Faradaic efficiency, current density, specific energy consumption, and single-pass conversion are used to compare electrolyzer performance across studies. In general, post-electrolysis product recovery requires complex separation of mixed ions, gases, and liquids. Because experimentally validated downstream separation processes remain limited, the economic and environmental performance of these systems remains uncertain. Overall, translating these laboratory successes into practical applications requires a broader, process-level perspective.

At the cell level, CO_2 reduction occurs at the cathode, whereas conventional electrolyzers use the oxygen evolution reaction (OER) at the anode. However, the high thermodynamic potential (i.e., 1.23 V) of OER typically consumes over 90% electricity required at the electrolyzer. Recently, researchers have explored replacing OER with other organic oxidation reactions (OORs) in coelectrolysis systems, eyeing on achieving higher economic potential and lower energy demand. Examples include oxidizing glycerol at the anode to produce lactic acid [20], oxidizing 5-hydroxymethyl-furfural to produce 2,5 furandicarboxylic [21], among others. While this coupling strategy provides inherent economic and energy benefits, the addition of new species and low selectivity make the challenges in downstream separation more severe. In addition, numerous combinations of ECO_2RR and OOR are possible. It would be very challenging and time-consuming to carry out detailed process design and evaluation on each combination to provide technical recommendations.

While previous reviews on low-temperature CO_2 electrolysis have often covered reactor design (including gas-diffusion electrodes, flow-cell and membrane electrode assembly design, mass transport, and scale up) [14,22], paired alternative anodic reactions [23–26], and process-level techno-economic considerations [27–29], they are typically organized by reaction type or catalyst and cell performance, with experimental data and downstream considerations treated separately. Consequently, a more integrated pre-design approach is needed.

To address this need, we introduce a conceptual design and integration framework for coelectrolysis systems pairing ECO_2RR (cathode) with OOR (anode). Drawing on reported experimental findings for both half-reactions, we propose a structured screening procedure. This framework evaluates inherent thermodynamic properties (e.g., theoretical voltage), technical performance metrics (e.g., current density, selectivity, specific energy consumption), and economic indicators (e.g., reactant and product unit costs) to identify combinations capable of sustaining the economic margins required for downstream separation processes. Ultimately, this study aims to connect process-level insights during the early design phase, identifying the most viable pathways for rigorous technical and economic evaluation.

2. Pairing of ECO_2RR and OOR

In this section, the potential ECO_2RR (cathode) and OOR (anode), as well as existing coelectrolysis systems, are reviewed. We aim to connect the fundamental properties of these electrochemical half reactions to broader process insights.

At the cathode, the target products of ECO_2RR are primarily determined by the choice of electrocatalyst. Table 1 summarizes the representative experimental data for various cathodic reduction pathways, where the types of electrocatalysts and electrolytes, information regarding the byproducts, and process indicators obtained from these experiments are listed. Generally, Faradaic efficiency (FE) and total current density (TCD) are used to evaluate electrochemical conversion systems. FE represents the fraction of charge directed toward the targeted product, reflecting the selectivity of the process. TCD denotes the overall rate of charge transfer per unit of electrode area. The product of FE and TCD, the partial current density, directly indicates the productivity of the electrochemical conversion. In contrast, the half-cell potential represents the electrical driving force required per unit charge. However, none of these indicators alone captures the electricity required per unit mass of product. Therefore, the specific electricity consumption (SEC), defined in Equation (1), is used here as the primary energy indicator for screening. For brevity, representative studies demonstrating high current density and Faradaic efficiency are listed for each chemical.

$$\mathrm{SEC} = \frac{|\mathrm{E_{half}}|\ \mathrm{nF}}{\mathrm{FE} \times \mathrm{M_p} \times 3.6 \times 10^6} \tag{1}$$

where E_{half} is the reported half-cell potential (vs. RHE), n denotes the number of electrons transferred per mole of product, F represents the Faraday constant, M_p is the product molar mass in kg mol^{-1}. Overall, SEC rises with the half-cell potential and reduces as FE increases. Although TCD does not appear explicitly in Equation (1), a higher

current density often requires larger half-cell-potentials or alters FE, thereby affecting SEC indirectly. Note that the SEC values listed in Table 1 describe cathodic half-reactions. The corresponding full-cell values for paired systems are used later in the economic evaluation.

Two key observations emerge from these data. First, controlling the selectivity of the reduction products remains a significant challenge. The competitive reduction of water to hydrogen frequently occurs at the cathode, further decreasing the overall selectivity toward the target carbon products. Second, while fundamental electrochemical principles dictate a trade-off between productivity and overpotential (as described by the Butler-Volmer equation), this is not a general trend across the various pathways listed in Table 1. Specifically, several systems for producing methanol and formate reveal higher partial current densities alongside lower SEC compared to others. This is particularly evident in formate production, which represents a widely investigated cathodic reaction pathway in the field of ECO_2RR. This phenomenon is driven by continued advancements in catalytic technologies (e.g., nanoparticle design and defect engineering).

Although downstream separation has not yet been considered, a preliminary economic margin can be estimated by comparing product revenue with the electricity cost implied by these SEC values. At an electricity price of \$0.10 kWh^{-1}, hydrocarbon production showed no positive margin and would require a substantial green premium to become profitable. In contrast, carbon monoxide, formate, and alcohol production showed positive preliminary margins and therefore warranted further evaluation, including detailed separation design.

The separation of individual products raises specific issues that require further investigation. For example, CO sometimes serves as a reaction intermediate in electrolyte systems, making it challenging to recover efficiently. Liquid products such as formic acid, ethanol, and propanol form azeotropes with water, which significantly complicates downstream separation processes. Furthermore, if the system produces liquid formate, an additional acidification step is required to convert it into its acid form before effective separation. Across all these pathways, the target chemicals must be separated from an aqueous electrolyte solution. Consequently, the proper recovery and recycling of the electrolytes is essential for the sustainability of the entire process.

At the anode, OORs should have a lower onset potential than the OER and yield products significantly more valuable than oxygen. Table 2 summarizes the representative OORs reported in the literature. Their onset potentials and Faradaic efficiencies serve as benchmarks to evaluate their feasibility for pairing with ECO_2RR. As indicated, the candidate products from OORs include various carboxylic acids, acetates, aldehydes and ketones. Most of these chemicals can be generated with a high Faradaic efficiency. The market prices of the target products, along with the costs of the corresponding organic reactants, are also provided to help identify the potential economic margin. However, from a process operation perspective, oxygen can be easily separated from the electrolyte solution, despite its lower economic value. This fundamental trade-off between product value and separation difficulties cannot be addressed by looking at the half-reaction alone.

Tables 1 and 2 independently assess the cathodic and anodic half-reactions in terms of their electrochemical performance, potential economic value, and separation considerations. Pairing these half-reactions, however, is not simply a matter of selecting the best entry from each table. In a full cell, the two electrodes are linked by charge balance, while the selected electrolyte environments and reactor architecture influence ion transport, species crossover, and outlet-stream composition. To illustrate these integrated effects, Table 3 summarizes representative existing full-cell coelectrolysis systems that integrate ECO_2RR and OOR. Formate/formic acid is the most common product, either generated from CO_2 reduction at the cathode or co-produced at the anode through glycerol, methanol, or ethylene glycol oxidation. Other reported product pairs include CO/FDCA, C_2H_4/FDCA, and C_2H_4/hypochlorite. Most systems operate in alkaline media, commonly KOH based electrolytes, with the anolyte containing the necessary organic substrates. Reactor configurations vary widely, encompassing flow cells, standard and zero-gap MEAs, membrane-free cells, and CEM-based flow cells. Overall, Table 3 illustrates how coelectrolysis research has progressed from isolated half-reactions toward integrated full-cell systems with diverse product combinations, electrolyte environments, and reactor designs.

Table 1. Representative data for half reactions at the cathode in the literature.

Products	Electrocatalyst	Electrolyte	Half-cell Potential (vs. RHE)	FE [a] (%)	TCD [b] (A/m^2)	SEC [c] (kWh/kg)	Market Price ($/kg)	Byproducts
CO	Ag nanoparticle [10]	1 M KOH	−1.60 V	83.5	2310	3.704	0.60	15% H_2; 1% $HCOO^-$
	Ni-S [30]	0.5 M $KHCO_3$	−0.62 V	98.0	325	1.223		H_2; others not reported
	Sn-NOC [31]	0.1 M $KHCO_3$	−0.7 V	94	148.1	1.425		HCOOH; H_2
CH_4	CuNCN-500 [32]	1 M KOH	−1.00 V	66.3	3000	5.091	0.02	20% H_2; 8% C_2H_5OH; 5% C_2H_6
	Zn [33]	1 M $KHCO_3$	−1.8 V	85.0	374	7.148		10% H_2; 3% CO
C_2H_4	CuNCN-300 [32]	1 M KOH	−1.00 V	48.5	5000	3.979		17% H_2; 10% CH_3COOH; 15% C_2H_5OH
	Cu cubes/spheres GDE [34]	1 M KOH	−0.7 V	60	2000	2.229		CO; H_2
MeOH	$Pd_{1.80\%}/MnO_2$ [9]	1 M KOH	−0.6 V	80.9	3010	1.253	0.32	10% CO; 10% H_2
	Mo_2C/N-CNT [35]	0.1 M $KHCO_3$	−1.10 V	80.4	40	2.312		10% H_2; 7% CO; 2% CH_4; 1% $HCOO^-$
FA	Sn(S)-H [11]	0.5 M K_2SO_4/H_2SO_4	N.A.	92.1	2000	——	0.73	5% CO; 3%H_2
Formate	$Sn_3O(OH)_2Cl_2$ [36]	0.5 M $KHCO_3$	−0.90 V	96.1	649	1.283		2% H_2; 2% CO
	Cu-doped SnS_2 [37]	0.5 M $KHCO_3$	−1.0 V	90.5	165	1.287		CO; H_2
	Sn(S)/Au needles [38]	0.1 M $KHCO_3$	−0.75 V	93.3	550	0.936		(CO, H_2) < 7%
	SnO_2 NP [39]	1 M $KHCO_3$	−1.21 V	64	1450	2.202		CO:16%; Ethanol:10%
	Ultra-small SnO_2 (grain-boundary rich) [39]	1 M KOH (flow cell)	−0.95 V	97	1000	1.141		CH_4:3%
Formate	hp-In (3D hierarchical [40] porous In)	0.1 M $KHCO_3$	−1.2 V	90.4	675	1.546		CO & H_2
	NTD-Bi (from Bi_2O_3 NTs) [41]	1 M $KHCO_3$	−0.86 V	90.4	1360	1.108		CO & H_2
	NTD-Bi (from Bi_2O_3 NTs) [41]	1 M KOH	−0.61 V	98	2880	0.725		CO & H_2
	Sn-SnSx on Cu foil (self-supporting) [42]	0.1 M $KHCO_3$ (CO_2-sat)	−1.2 V	93.3	199	1.498		CO:3%; H_2:4%
	POD-Bi (p-orbital delocalized Bi) [43]	0.5 M $KHCO_3$	−0.61 V	93	2000	0.764		CO & H_2
C_2H_6	CuI [44]	0.1 M $NaHCO_3$	−0.74 V	30.0	200	4.441	0.02	30% H_2; 11% C_2H_4; 9% C_2H_5OH; 7% CO; 5% $HCOO^-$; 5% C_3H_7OH
EtOH	SnS_2/Single atom Sn [12]	0.5 M $KHCO_3$	−0.90 V	82.5	178	1.336	1.18	15% $HCOO^-$; 5% CO; 3% H_2
	$CuSn_{0.025}$ [45]	0.1 M $KHCO_3$	−1.40 V	26	580	6.265		H_2:13%; CO:7%; CH_4:10%; C_2H_4:33%
n-PrOH	$Ag_{0.015}In_{0.985}Se_{0.734}$ [46]	0.1 M $KHCO_3$	−0.60 V	75.2	134	0.719	0.83	15% CO; 10% H_2
Propene	Cu nanoparticle [47]	1 M KOH + 0.2 M CsI	−0.60 V	1.42	2863	54.22	0.88	50.85% C_2H_4; 15.95% C_2H_5OH; 15.36% H_2; 7.21% CO; 4.12% C_3H_7OH; 2.19% $HCOO^-$; 0.68% CH_3COO^-; 0.42% C_3H_6O; 0.14% CH_4; 0.02% C_2H_6

[a] FE: faradic efficiency; [b] TCD: total current density; [c] SEC: specific electricity consumption.

Table 2. Representative data for half reactions at the anode in the literature.

Reactant	Product	Half-Reaction	Potential (V)	FE%	Material Cost ($/kg)	Prod. Market Price ($/kg)
Water	Oxygen	$2H_2O \rightarrow O_2+4H^++4e^-$	1.600	100% [29]	0.000	0.223
Water	Hydrogen Peroxide	$2H_2O \rightarrow H_2O_2+2H^++2e^-$	2.500	35% [48]	0.000	0.505
Methanol	Formaldehyde	Methanol→ Formaldehyde+$2H^++2e^-$	0.505	47% [49]	0.753	0.503
Methanol	Formic Acid	Methanol+$H_2O \rightarrow$ Formic Acid+$4H^++4e^-$	0.502	~100% [50]	0.753	0.930
Methanol	Formic Acid	Methanol+$H_2O \rightarrow$ Formic Acid+$4H^++4e^-$	1.654	>98% [51]	0.753	0.930
Ethanol	Acetaldehyde	Ethanol → Acetaldehyde+$2H^++2e^-$	1.453	89% [52]	0.960	1.080
Ethanol	Acetic Acid	Ethanol+$H_2O \rightarrow$ Acetic Acid+$4H^++4e^-$	1.446	73% [53]	0.960	0.572
Ethanol	Ethyl Acetate	2Ethanol → Ethyl Acetate+$4H^++4e^-$	1.322	98% [54]	0.960	1.184
Ethylene Glycol	Glycolic Acid	Ethylene Glycol+$H_2O \rightarrow$ Glycolic Acid +$4H^++4e^-$	0.336	85% [55]	0.665	1.500
Ethylene Glycol	Oxalic Acid	Ethylene Glycol+$2H_2O \rightarrow$ Oxalic Acid +$8H^++8e^-$	0.345	60% [56]	0.665	1.310
Ethylene Glycol	Glycolic Acid	Ethylene Glycol+$H_2O \rightarrow$ Glycolic Acid +$4H^++4e^-$	1.250	93% [57]	0.665	1.500
Isopropanol	Acetone	Isopropanol+$H_2O \rightarrow$ Acetone+$2H^++2e^-$	1.354	98% [58]	1.270	1.045
Glycerol	Lactic Acid	Glycerol → Lactic Acid+$2H^++2e^-$	0.451	73% [59]	1.148	1.100
1,3-Propanediol	Acrylic Acid	1,3-Propanediol → Acrylic Acid+$4H^++4e^-$	0.798	77% [60]	4.126	1.453
1,2-Propanediol	Lactic Acid	1,2-Propanediol+$H_2O \rightarrow$ Lactic Acid+ $4H^++4e^-$	0.486	87% [61]	1.728	1.100
Benzyl Alcohol	Benzaldehyde	Benzyl Alcohol → Benzaldehyde+$2H^++2e^-$	1.203	96% [62]	1.978	1.465
Benzyl Alcohol	Benzoic Acid	Benzyl Alcohol+$H_2O \rightarrow$ Benzoic Acid +$4H^++4e^-$	1.046	98% [63]	1.978	1.465
Furfural	Furoic Acid	Furfural+$H_2O \rightarrow$ Furoic Acid+$2H^++2e^-$	1.430	~100% [64]	1.665	131.88
Furfuryl Alcohol	Furoic Acid	Furfuryl Alcohol+$H_2O \rightarrow$ Furoic Acid +$4H^++4e^-$	1.365	~100% [65]	1.720	131.88
5-Hydroxymethylfurfural (HMF)	2,5-Furandicarboxylic Acid (FDCA)	HMF +$H_2O \rightarrow$ FDCA +$6H^++6e^-$	1.250	99% [21]	440	600

Table 3. Representative coelectrolysis systems reported in the literature.

Authors	Electrode	Electrocatalyst	Electrolyte	Reactant	Product	FE (%)	E (V)	CD (A m^{-2})	Time (hr)	Type of Electrolyzer
Chen et al. [66]	Cathode	Bi NS/carbon paper	1 M KOH	CO_2	Formate	91.3	2.32	1600	10	MEA
	Anode	NiOOH@Ni_3S_2/NF	1 M KOH + 0.3M Glycerol	Glycerol	Formate	98.7				
Li et al. [67]	Cathode	Bi_2O_3	1 M KOH + 0.5 M Glycerol	CO_2	Formate	96.0	2.25	1000	313	Without membrane
	Anode	NiV/Ni foam		Glycerol	Formate	97.0				
Le et al. [68]	Cathode	Sn/Sigracet 39BB	1 M KOH	CO_2	Formate	85.0	2.55	500	100	flow cell
	Anode	CNBO	1 M KOH + 0.1 M Glycerol	Glycerol	Formate	89.6				
Lu et al. [69]	Cathode	Ni/Fe-DAC	1M KOH	CO_2	CO	100	1.48	2000	-	Flow cell
	Anode	Pd-NF	1 M KOH + 0.1 M HMF	HMF	FDCA	90				
Liu et al. [70]	Cathode	Cu_1Bi	1 M KOH	CO_2	Formate	90	2.35	1500	10	MEA
	Anode	NiCoLDH/NF	1 M KOH + 0.1 M HMF	HMF	FDCA	85				
Zhang et al. [71]	Cathode	Cu_2O/CuNF@GDL	0.5 M KCl	CO_2	C_2H_4	74.5	2.75	1888	5	flow cell
	Anode	CuO-NF@Cu	2 M KOH + 0.01 M HMF	HMF	FDCA	96.6				
Zhou et al. [72]	Cathode	Ni&NiNC	1 M KOH	CO_2	formate	90.0	2.4	5000	8	Zero gap–MEA
	Anode	Ni-MOFs@350	1 M KOH + 1 M Methanol	Methanol	Formate	90.0				

Table 3. *Cont.*

Authors	Electrode	Electrocatalyst	Electrolyte	Reactant	Product	FE (%)	E (V)	CD (A m^{-2})	Time (hr)	Type of Electrolyzer
Kang et al. [73]	Cathode	in situ-formed Cu/GDL	0.5 M KOH + 1.5 M sea salt + 1 mg/mL EDTA	CO_2	C_2H_4	47.0	-	1000	3	Flow cell
	Anode	GDL	0.5 M KOH + 1.5 M sea salt + 1 mg/mL EDTA	Sea salt	ClO^-	85.0				
Yu et al. [74]	Cathode	$Bi_2O_2CO_3$@GDE	1 M KOH	CO_2	Formate	86.0	3.4–4.0	5000	100	Flow cell
	Anode	3D Ni foam	1 M KOH + ethylene glycol	Ethylene glycol	Formate	93.7				
Pei et al. [75]	Cathode	BiOI/CP	0.5 M $KHCO_3$	CO_2	Formate	92	1.9	224	-	Two-electrode cell
	Anode	$Ni_{0.33}Co_{0.67}(OH)_2$	1 M KOH + 0.1 M glycerol	Glycerol	Formate	90				
Wang et al. [76]	Cathode	Ag/GDL	3 M KCl, pH 1 by H_2SO_4	CO_2	CO	96	3.2	1000	10	CEM flow cell
	Anode	Pt/Ti fiber felt	0.05 M KOH + 0.5 M allyl alcohol	Allyl alcohol	Acrolein	85				
Zhang et al. [77]	Cathode	NiPc-NiPor COF	0.5 M $KHCO_3$	CO_2	CO	98.12	2.1	62	8.5	Two electrode cell
	Anode		1 M KOH + 1 M methanol	Methanol	HCOOH	93.75				
Vehrenberg et al. [78]	Cathode	Sn/C GDE	0.5 M $KHCO_3$	CO_2	Formate	74	4.4	500	5	CEM flow cell
	Anode	Pt/C	1 M KOH + 2 M glycerol	Glycerol	Formate	30				

3. Process Perspectives

3.1. Rationale for Process Screening

Figure 1 depicts the conceptual flowchart for designing the co-electrolysis process. It consists of four steps: half-reaction mapping and shortlisting (Step 1), preliminary gross-margin evaluation (Step 2), detailed process simulation (Step 3), and final process-level comparison (Step 4). Given the multitude of half-reactions occurring at the anode and cathode, it is very inefficient to conduct detailed simulations for every possible combination. Here, we propose a screening framework for early-stage decision-making (i.e., Steps 1 and 2 in Figure 1). This tool first screens out reaction pairs that are impractical for coupled electrolyzers, and then identifies the remaining candidates that warrant detailed process simulation based on their economic margins.

In Step 1, the reported data for current density, Faradaic efficiency, and potential are used to construct technology feasibility maps for individual OOR (anodic) and ECO_2RR (cathodic). Here, we specifically focused on the partial current density that used to produce the targeted product, which was derived from the reported current density and Faradaic efficiency.

Table 4 presents the minimum industrial standards published by the Fraunhofer Society for the electrochemical conversion of CO_2. Although specifically discussing carbon monoxide, formic acid, and ethylene, these metrics provide a valuable baseline for evaluating the industrial potential of various lab-scale technologies. Practical industrial requirements often deviate from laboratory-scale conditions in several key aspects. First, balancing productivity and energy efficiency requires a minimum current density of 200 mA/cm^2 and electrolyzer voltage below 3 V. Second, industrial systems must operate between 60 and 90 °C, which is significantly higher than the temperature in typical room-temperature experiments. This elevated temperature is process-driven, aiming to reduce cooling costs, lower solution resistance, and accelerate carbon dioxide mass transfer. Finally, the heat generated from electrical energy dissipation lowers the overall energy efficiency. However, it is challenging to accurately measure this heat release in lab-scale experiments. Therefore, crucial parameters such as electrode stability, membrane durability, and reaction selectivity under actual high-temperature operations still require rigorous verification to successfully meet industrial expectations.

Table 4. The minimum requirements and latest technologies for the industrial application of electrochemical conversion [79].

Items	Minimum Requirement	Latest Technology
Current density	>200 mA/cm^2	500–1800 mA/cm^2
Energy efficiency	>50%	~40% [80]
Faradaic efficiency	>80%	80–90%
Voltage (@300 mA/cm^2)	<3.0 V (Note: better < 2.5 V; ideal < 2.0 V)	2.7 V
Per-pass conversion	>50%	30–70%
Operating temperature	60–90 °C [81]	40–80 °C
Other Challenges		
Stability	<10 μV h^{-1}	
Electricity cost	<0.04 $/kWh [8]	
Membrane selection	Currently using anion exchange membrane (AEM), targeting for bipolar membrane (BPM) for better efficiency	
Inlet concentration	CO_2 > 10 vol%, deep removal of NO_x and O_2 [82,83]	

Figure 2a,b illustrate the technology feasibility screening results (Step 1) for OORs and ECO_2RR, respectively. Both scatter plots display the potential (y-axis) and the partial current density (x-axis) of the existing studies in literature. Based on the requirements listed in Table 4, we identified the threshold of 0.16 A cm^{-2} for partial current density (derived from a total current density of 200 mA cm^{-2} and a Faradaic efficiency of 80%), and 2.0 V potential for each reaction. This establishes an early-stage screening window, and all the candidates passing this screening are sent to the next step. Among these candidates, the representative paired cases summarized in Table 5 were constructed by matching half-reactions with compatible alkaline or carbonate electrolyte environments, comparable operating conditions, and sufficient reported data for charge-balance and margin calculations.

In Step 2, economic margins are calculated for the half-reaction pairings that passed the initial screening. The margin for each combination is determined by subtracting total reactant and electricity costs from the combined revenues of the anodic and cathodic products. Table 5 summarizes these results for representative pairings, all normalized to a basis of 1 kg of cathodic product. Because most literature focuses on cathodic ECO_2RR metrics,

the corresponding anodic reactants and products are derived via charge balance. The total electricity requirement is evaluated based on the specific electricity consumption (SEC) per kilogram of cathodic product, assuming an electricity cost of 0.10 $/kWh. Ultimately, pairings with negative gross margins lack the necessary economic allowance to offset downstream separation costs and are therefore screened out.

Table 5 reveals that seven of the nine evaluated pairings exhibit positive economic margins, predominantly ranging from $0.1/kg to $0.4/kg. Notably, Cases #5 and #6, which couple cathodic methanol production with anodic glycolic acid production (via ethylene glycol oxidation), yield the highest gross margins (>$2.0/kg), making them highly recommended for detailed process design. On the other hand, while Cases #1 and #2 present lower economic margins, they generate identical products (formate) at both electrodes. This unique feature significantly simplifies downstream separation. Therefore, despite the smaller economic margins, the potential of pairing half-reactions to co-produce the same product should not be overlooked.

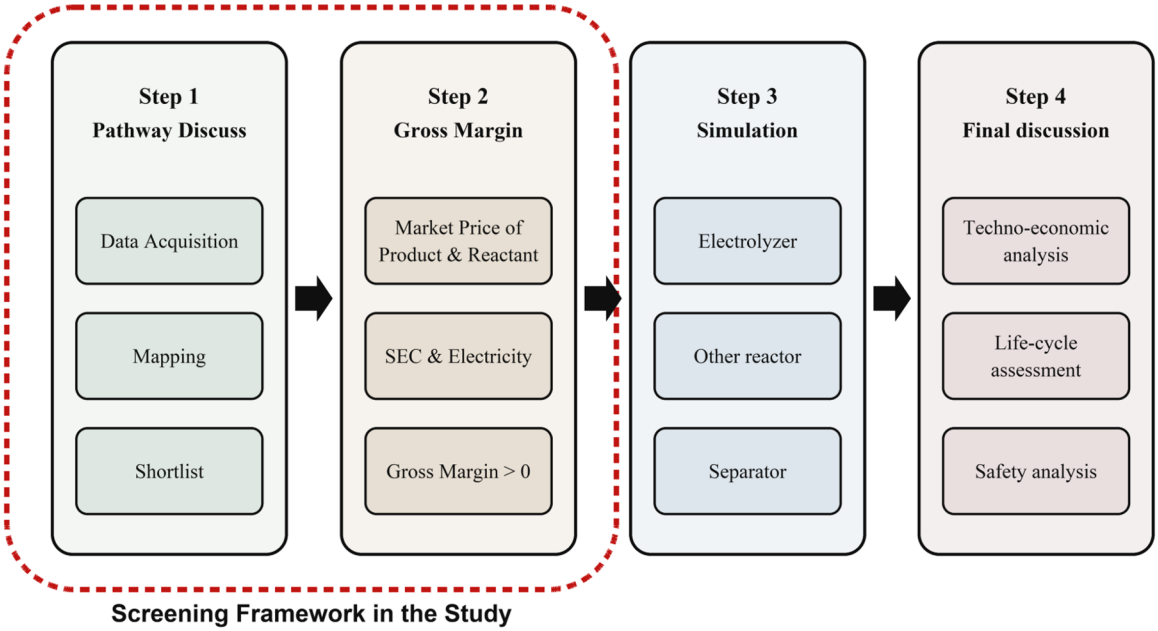

Figure 1. The concept of the screening framework proposed in this study.

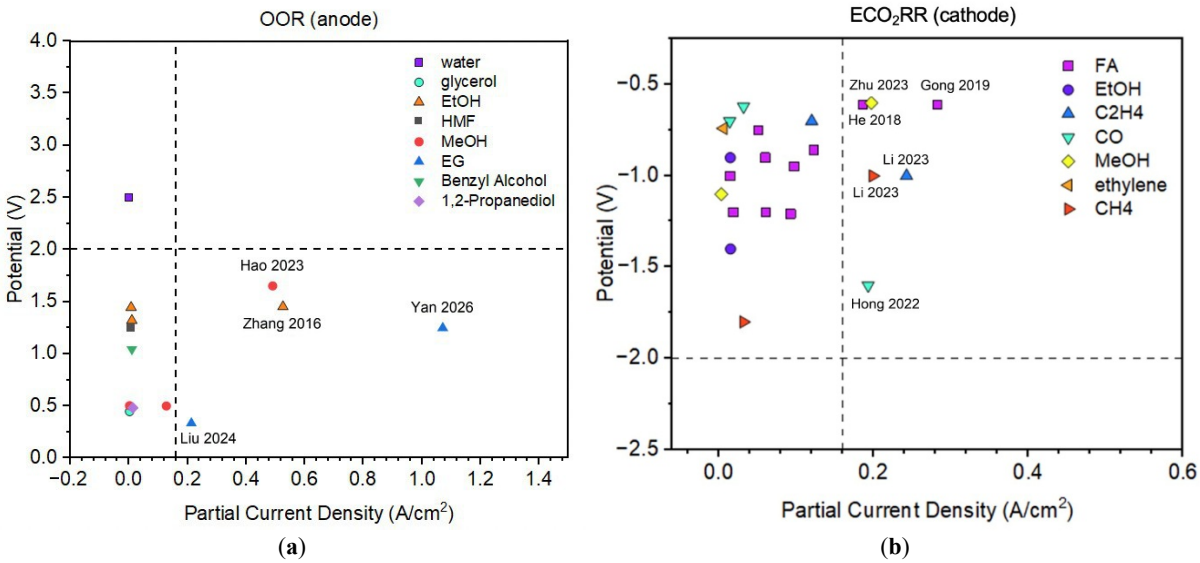

Figure 2. The screening results. (**a**) anode; (**b**) cathode. Points are labelled by first author and year: (**a**) Hao 2023 [51], Zhang 2016 [52], Liu 2024 [55] and Yan 2026 [57]; (**b**) Zhu 2023 [9], Hong 2022 [10], Li 2023 [32] (two points), Gong 2019 [41] and He 2018 [43].

Table 5. Results for economic margins for the candidate paired electrolysis systems.

Case	Electrode	Electrolyte	Main Product	Revenue * ($/kg)	SEC * (kWh/kg)	Gross Margin * ($/kg)	Ref.
#1	Cathode	1 M KOH	Formate	0.435	2.691	0.166	[41,51]
	Anode	1 M KOH + 1 M MeOH	Formate				
#2	Cathode	0.5M $KHCO_3$	Formate	0.446	2.835	0.162	[43,51]
	Anode	1 M KOH + 1 M MeOH	Formate				
#3	Cathode	1M KOH	CO	0.776	4.437	0.332	[10,55]
	Anode	1 M NaOH + 1 M EG	Glycolic acid				
#4	Cathode	1 M KOH	CO	0.900	6.532	0.247	[10,57]
	Anode	3 M KOH + 0.3 M EG	Glycolic acid				
#5	Cathode	1 M KOH	MeOH	2.898	5.807	2.318	[9,55]
	Anode	1 M NaOH + 1 M EG	Glycolic acid				
#6	Cathode	1 M KOH	MeOH	3.235	11.477	2.088	[9,57]
	Anode	3 M KOH + 0.3 M EG	Glycolic acid				
#7	Cathode	1 M KOH	CO	−0.156	7.458	−0.901	[10,51]
	Anode	1 M KOH + 1 M MeOH	Formate				
#8	Cathode	1 M KOH	MeOH	0.376	13.983	−1.022	[9,51]
	Anode	1 M KOH + 1 M MeOH	Formate				
#9	Cathode	1 M KOH	Formate	0.823	4.270	0.396	[84]
	Anode	0.5 M KOH + 1 M EtOH	Acetate				

***** Calculate on producing 1 kg cathodic product.

The reaction pairs shortlisted in Table 5 still require validation at larger scales. Larger-area cells and stacks must meet the Table 4 targets [79,81] while maintaining performance at both electrodes and managing reactant and electrolyte flows, current distribution, water and heat, and product crossover [85]. Future studies should report full-cell voltage, Faradaic efficiency and productivity at both electrodes, single-pass conversion, product concentration, crossover, and material balances during continuous operation. These data are needed for separation design and techno-economic and life-cycle assessment.

3.2. The Separation Strategies

Product separation from aqueous electrolytes constitutes a considerable challenge. Due to the low product concentrations in the electrolyzer output, the separation process often entails a significant energy penalty, with the energy required for purification being substantially higher relative to the electrolysis itself. Generally, using the boiling point of water as a reference, the hierarchy of separation difficulty is as follows: ionic species are the most challenging to recover, followed by high boiling azeotropes, high boiling compounds, low boiling azeotropes, and finally low boiling compounds. Additionally, the phenomenon of crossover [85], wherein products or ions migrate across the membrane, results in further product loss and electrolyte contamination. These factors, coupled with the presence of various byproducts, markedly increase the complexity of downstream purification and affect the overall feasibility of the system.

Most systems that pass the screening utilize alkaline electrolytes, where acidic products typically exist in their ionic salt forms. For these specific scenarios, the conversion of these ions back into their neutral acid forms can be achieved through either chemical acidification followed by evaporation or bipolar membrane electrodialysis. While chemical acidification is a straightforward approach that requires the addition of a strong acid, bipolar membrane electrodialysis utilizes electrical energy to split water and directly acidify the product stream, avoiding the need for external chemical reagents. The choice between these two methods involves a clear trade-off: chemical acidification is simpler but increases operational costs owing to reagent consumption, whereas bipolar membrane electrodialysis is more elegant but requires a higher capital investment in specialized membrane equipment.

However, bipolar membrane electrodialysis is not without limitations, as ion crossover can significantly hinder its performance [86]. When product ions unintentionally migrate across the membrane, an additional acid or base must be introduced to neutralize the stream. This process inadvertently converts the target molecules back to salts, necessitating a subsequent evaporation step (e.g., multi-effect evaporation) to recover the final product. In such cases, the process essentially resembles a more complex and energy-intensive version of chemical acidification. Furthermore, this unintended ion migration and the resulting neutralization requirements lead to a sharp increase in the electricity demand. This additional energy consumption incurs a substantial penalty that negatively impacts the economic and environmental performance of the overall system.

Once the products are recovered from their ionic forms, the focus shifts to their purification and concentration from dilute aqueous solutions. Distillation is a primary method for separating zeotropic systems. However, the

presence of azeotropes introduces significant complexity (e.g., the maximum boiling azeotrope such as formic acid and water, or minimum boiling azeotropes such as ethanol and propanol in water). Therefore, advanced techniques (e.g., pressure swing distillation, extractive distillation, or hybrid extraction-distillation) must be employed [87–89]. The separation challenge is further intensified when byproducts are present, even in small amounts, as they can form additional multicomponent azeotropes that require even more sophisticated and energy intensive recovery strategies. Overall, the energy penalty associated with these distillation processes is highly sensitive to the initial product concentration. In dilute systems, the heat duty required to vaporize large amounts of water or to maintain high reflux ratios can become the dominant factor in the overall operational cost, potentially overshadowing the energy savings achieved in the electrolyzer.

Taken together, the evidence in Tables 1–3, the scale-up targets in Table 4, the screening results in Table 5, and the separation analysis presented above show that reported half-cell performance alone does not determine whether a pairing warrants further development. The two electrodes must satisfy charge balance under compatible operating conditions, and a positive preliminary gross margin must leave sufficient allowance for downstream recovery and purification costs. Figure 3 places these requirements in historical context. Paired ECO_2RR–OOR systems build on early studies of electrochemical CO_2 reduction and electrode-dependent product selectivity [90,91]. Later work demonstrated that the oxygen evolution reaction could be replaced by value-added alcohol oxidation [92,93] and expanded the analysis from individual electrodes to the process-level evaluation and screening of candidate reaction pairs [20,29]. Subsequent studies reported durable paired operation and reactant recycle [94,95], followed by high-rate operation and product management [72,96,97]. More recent studies reported enlarged-cell operation and large-area membrane-electrode-assembly stack demonstrations [67,98]. Because these milestones involve different reaction pairs and operating conditions, Figure 3 traces the broadening of development priorities rather than a year-by-year performance trend. Section 3.3 then illustrates how reaction pairing, product recovery, and process-level evaluation are combined in a single process.

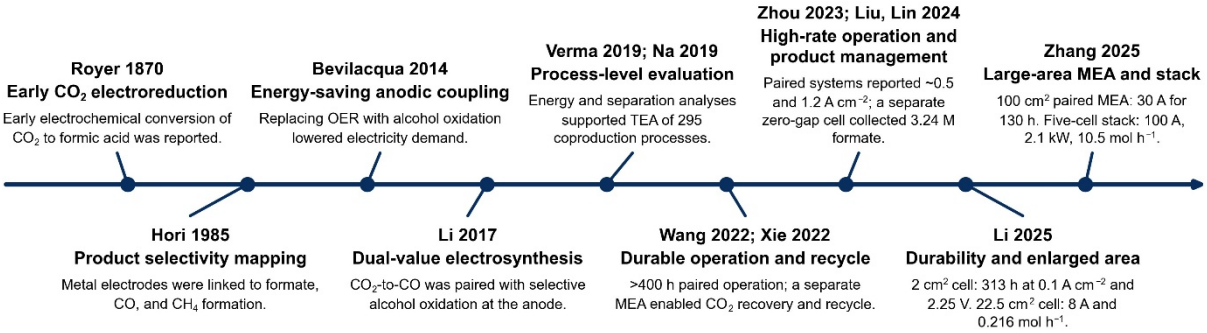

Figure 3. Selected milestones leading to and within paired ECO_2RR–OOR systems, from early electrochemical CO_2 reduction and product-selectivity mapping to recent demonstrations of durable high-rate operation, product management, enlarged cells, and large-area MEA stacks. Milestones are labelled by first author and year: Royer 1870 [91]; Hori 1985 [90]; Bevilacqua 2014 [92]; Li 2017 [93]; Verma 2019 [20] and Na 2019 [29]; Wang 2022 [94] and Xie 2022 [95]; Zhou 2023 [72], Liu 2024 [96] and Lin 2024 [97]; Li 2025 [67]; Zhang 2025 [98].

3.3. An Example for a Complete Electrochemical CO_2 Conversion Process

Our group has investigated a coelectrolysis system for the simultaneous conversion of CO_2 and ethanol into formate and acetate (i.e., Case #9 in Table 5) [84]. The integrated process begins with monoethanolamine-based carbon capture to provide a high-purity feedstock for the system. In an alkaline electrolyzer, CO_2 is reduced to formate at the cathode, while ethanol is oxidized to acetate at the anode. This coupling of ethanol oxidation at the anode helps reduce the voltage of the electrolyzer. This stage is followed by bipolar membrane electrodialysis (BPMED) for the acidification and recovery of these ions in their corresponding neutral acid forms (i.e., acetic acid from the anode, and formic acid from the cathode). The downstream section then employs a distillation sequence to concentrate formic acid to 85 weight percent and a hybrid extraction distillation process to purify acetic acid to 99 weight percent. Furthermore, potassium sulfate, which is generated as a byproduct of ion migration within the electrodialysis unit, is recovered through multi-effect evaporation and crystallization. The overall process concept is depicted in Figure 4.

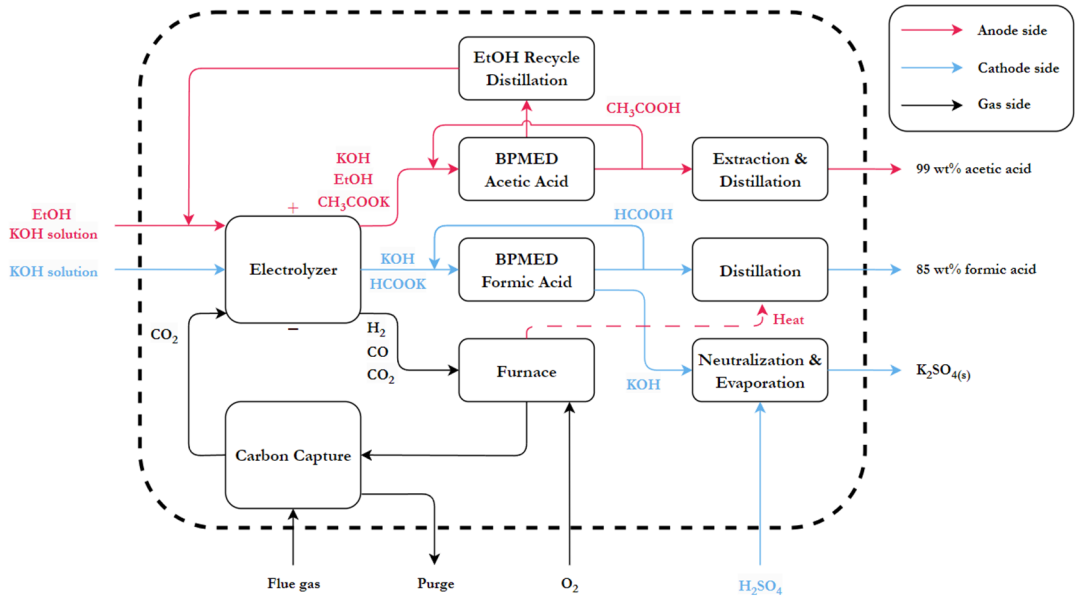

Figure 4. The overall process concept of the coelectrolysis process involving ethanol (anode) and CO_2 (cathode).

The baseline evaluation of this integrated system initially showed a global warming potential (GWP) of 16.87 kg CO_2eq per kg of formic acid and a minimum selling price (MSP) of $6.94/kg [84]. To address these economic and environmental barriers, several strategic optimizations have been explored, including the adoption of solar photovoltaic energy to eliminate the grid carbon footprint, elimination of acid crossover within the bipolar membrane, reduction of electrolyzer voltage, and lowering of capital investment. Under these optimized conditions, the GWP and MSP significantly decreased to 0.94 kg CO_2eq and $1.39/kg, respectively. While further experimental verification of this integrated process remains necessary, these results provide quantitative economic and environmental profiles for the investigated coelectrolysis process.

4. Conclusions

This paper reviewed the progress of ECO_2RR and OOR and proposed a framework to screen for potential coelectrolysis systems. We aimed to connect technological performance (e.g., current density, Faradaic efficiency, and operating potential) reported in the literature with economic margins, which are used to shortlist possible combinations. Due to the numerous possible combinations of half-reactions, this framework helps identify the potential combinations before conducting detailed process design.

Overall, we conclude that paired CO_2 electrolysis is economically viable when the added value from the anodic reaction provides sufficient margins to offset downstream separation and purification costs (e.g., pairing MeOH and glycolic acid production), or when both half-reactions yield identical products (e.g., formate), which potentially simplifies downstream processing. We introduced the detailed engineering concept using a demonstrative coelectrolysis system coupling CO_2 reduction with ethanol oxidation. Evaluating its baseline and prospective economic and environmental profiles allowed us to identify process bottlenecks and characterize potential improvements.

In summary, this screening framework enables early-stage decision-making for coelectrolysis systems. Future research must shift from optimizing isolated electrochemical metrics to generating process-relevant data (e.g., outlet stream composition, crossover, carbon balance, and long-term stability), which is crucial for designing downstream separation and conducting reliable techno-economic and life-cycle analyses. Ultimately, coupled CO_2 electrolysis will only achieve practical viability when reaction pairing, electrolyte management, and separation strategies are optimized together as an integrated process.

Author Contributions: K.-W.C.: investigation, methodology, data curation, writing—original draft preparation, writing—reviewing and editing; C.-H.L.: conceptualization, investigation, methodology, data curation; B.-Y.Y.: conceptualization, methodology, writing—original draft preparation, writing—reviewing and editing, supervision.

Funding: The research funding from National Science and Technology Council of R. O. C. (grant number: 114-2221-E-002-199-MY2, 114-2218-E-002-019, and 114-2923-E-006-004) is greatly appreciated.

Institutional Review Board Statement: Not applicable.

Informed Consent Statement: Not applicable.

Data Availability Statement: Not applicable.

Conflicts of Interest: The authors declare no conflict of interest.

Use of AI and AI-Assisted Technologies: During the preparation of this work, the authors used Paperpal to proofread our manuscript. After using this tool, the authors reviewed and edited the content as needed and take full responsibility for the content of the published article.

References

1. Chiu, H.H.; Yu, B.Y. Synthesis of green light olefins from direct hydrogenation of CO_2. Part I: Techno-economic, decarbonization, and sustainability analyses based on rigorous simulation. *J. Taiwan. Inst. Chem. E* **2024**, *156*, 105340.
2. Chiu, H.H.; Yu, B.Y. Synthesis of green light olefins from direct hydrogenation of CO_2. Part II: Detailed process design and optimization. *J. Taiwan Inst. Chem. E* **2024**, *155*, 105287.
3. Lee, M.T.; Chiu, H.H.; Yu, B.Y. Exploration of environmentally friendly processes for converting CO_2 into propanol through direct hydrogenation. *J. Ind. Eng. Chem.* **2025**, *143*, 271–282.
4. Wu, P.J.; Hsu, C.C.; Yu, B.Y.; et al. Rigorous simulation and comprehensive analysis for the novel glycerol carbonate (GC) production process via indirect conversion of CO_2. *Fuel* **2024**, *357*, 129831.
5. Huang, T.H.; Chen, Y.S.; Yu, B.Y. Techno-economic, environmental, and exergetic evaluation of a novel isopropyl n-phenylcarbamate production process through non-reductive conversion of CO_2. *Process Saf. Environ.* **2023**, *179*, 124–136.
6. Su, T.-E.; Chen, Y.-X.; Huang, T.-W.; et al. Current progress, potentials, and challenges for developing photo-assisted CO_2 conversion processes. *Camb. Prism. Carbon. Technol.* **2025**, *1*, e7.
7. Yin, Z.; Sun, H.; Li, W.; et al. Rational design of photocatalysts for CO_2 reduction to multi-carbon products. *Nano-Electrochem. Nano-Photochem.* **2025**, *1*, 6.
8. De Luna, P.; Hahn, C.; Higgins, D.; et al. What would it take for renewably powered electrosynthesis to displace petrochemical processes? *Science* **2019**, *364*, eaav3506.
9. Zhu, N.; Zhang, X.; Chen, N.; et al. Integration of MnO_2 nanosheets with Pd nanoparticles for efficient CO_2 electroreduction to methanol in membrane electrode assembly electrolyzers. *J. Am. Chem. Soc.* **2023**, *145*, 24852–24861.
10. Hong, J.; Park, K.T.; Kim, Y.E.; et al. Ag/C composite catalysts derived from spray pyrolysis for efficient electrochemical CO_2 reduction. *Chem. Eng. J.* **2022**, *431*, 133384.
11. Shen, H.; Jin, H.; Li, H.; et al. Acidic CO_2-to-HCOOH electrolysis with industrial-level current on phase engineered tin sulfide. *Nat. Commun.* **2023**, *14*, 2843.
12. Ding, J.; Yang, H.B.; Ma, X.-L.; et al. A tin-based tandem electrocatalyst for CO_2 reduction to ethanol with 80% selectivity. *Nat. Energy* **2023**, *8*, 1386–1394.
13. Hauch, A.; Küngas, R.; Blennow, P.; et al. Recent advances in solid oxide cell technology for electrolysis. *Science* **2020**, *370*, eaba6118.
14. Wakerley, D.; Lamaison, S.; Wicks, J.; et al. Gas diffusion electrodes, reactor designs and key metrics of low-temperature CO_2 electrolysers. *Nat. Energy* **2022**, *7*, 130–143.
15. Masel, R.I.; Liu, Z.; Yang, H.; et al. An industrial perspective on catalysts for low-temperature CO_2 electrolysis. *Nat. Nanotechnol.* **2021**, *16*, 118–128.
16. Shin, H.; Hansen, K.U.; Jiao, F. Techno-economic assessment of low-temperature carbon dioxide electrolysis. *Nat. Sustain.* **2021**, *4*, 911–919.
17. Li, X.; Chen, Y.; Zhan, X.; et al. Strategies for enhancing electrochemical CO_2 reduction to multi-carbon fuels on copper. *Innov. Mater.* **2023**, *1*, 100014.
18. Duanmu, J.-W.; Yang, X.-P.; Gao, F.-Y.; et al. Progress of mechanistic pathways involved in electrochemical CO_2 reduction. *J. Energy Chem.* **2025**, *102*, 745–767.
19. Xie, L.; Liu, Y.; Li, S.; et al. Phase and facet engineering for nanoscale catalyst discovery in electrochemical CO_2 reduction. *Nat. Synth.* **2026**, *5*, 489–505.
20. Verma, S.; Lu, S.; Kenis, P.J. Co-electrolysis of CO_2 and glycerol as a pathway to carbon chemicals with improved technoeconomics due to low electricity consumption. *Nat. Energy* **2019**, *4*, 466–474.
21. Liu, W.-J.; Dang, L.; Xu, Z.; et al. Electrochemical oxidation of 5-hydroxymethylfurfural with NiFe layered double hydroxide (LDH) nanosheet catalysts. *ACS Catal.* **2018**, *8*, 5533–5541.
22. Ma, D.; Jin, T.; Xie, K.; et al. An overview of flow cell architecture design and optimization for electrochemical CO_2 reduction. *J. Mater. Chem. A* **2021**, *9*, 20897–20918.
23. Chen, H.; Ding, C.; Kang, C.; et al. The design of alternative anodic reactions paired with electrochemical CO_2 reduction. *Green. Chem.* **2023**, *25*, 5320–5337.

24. Li, D.; Yang, J.; Lian, J.; et al. Recent advances in paired electrolysis coupling CO_2 reduction with alternative oxidation reactions. *J. Energy Chem.* **2023**, *77*, 406–419.
25. Xu, Z.; Peng, C.; Zheng, G. Coupling value-added anodic reactions with electrocatalytic CO_2 reduction. *Chem. –A Eur. J.* **2023**, *29*, e202203147.
26. Li, Y.; Lu, T.-B. Coupling electrochemical CO_2 reduction with value-added anodic oxidation reactions: Progress and challenges. *Mater. Chem. Front.* **2024**, *8*, 341–353.
27. Zhai, Y.; Wang, C.; Chen, Z. System design in CO_2 electrolysis: Integrating value-added anode reactions with cathodic reduction. *Molecules* **2025**, *30*, 4485.
28. Jiang, C.; Zhang, Z.; Deuss, P.J.; et al. CO_2 electroreduction coupled with the electrooxidation of alcohols and sugars to formate: Review and evaluation. *ChemSusChem* **2025**, *18*, e202500478.
29. Na, J.; Seo, B.; Kim, J.; et al. General technoeconomic analysis for electrochemical coproduction coupling carbon dioxide reduction with organic oxidation. *Nat. Commun.* **2019**, *10*, 5193.
30. Sun, X.; Wang, L.; Lan, X.; et al. Positively charged nickel-sulfur dual sites for efficient CO_2 electroreduction reaction. *Appl. Catal. B Environ.* **2024**, *342*, 123389.
31. Guo, J.; Zhang, W.; Zhang, L.-H.; et al. Control over electrochemical CO_2 reduction selectivity by coordination engineering of tin single-atom catalysts. *Adv. Sci.* **2021**, *8*, 2102884.
32. Li, H.; Cao, S.; Sun, H.; et al. CuNCN derived Cu-based/C_xN_γ catalysts for highly selective CO_2 electroreduction to hydrocarbons. *Appl. Catal. B Environ.* **2023**, *320*, 121948.
33. Han, L.; Song, S.; Liu, M.; et al. Stable and Efficient Single-Atom Zn Catalyst for CO_2 Reduction to CH_4. *J. Am. Chem. Soc.* **2020**, *142*, 12563–12567.
34. De Gregorio, G.L.; Burdyny, T.; Loiudice, A.; et al. Facet-dependent selectivity of Cu catalysts in electrochemical CO_2 reduction at commercially viable current densities. *ACS Catal.* **2020**, *10*, 4854–4862.
35. Zhang, G.; Wang, T.; Zhang, M.; et al. Selective CO_2 electroreduction to methanol via enhanced oxygen bonding. *Nat. Commun.* **2022**, *13*, 7768.
36. Wang, T.; Chen, J.; Ren, X.; et al. Halogen-incorporated Sn catalysts for selective electrochemical CO_2 reduction to formate. *Angew. Chem. Int. Ed.* **2023**, *62*, e202211174.
37. Chen, M.; Wan, S.; Zhong, L.; et al. Dynamic restructuring of Cu-Doped SnS_2 Nanoflowers for highly selective electrochemical CO_2 reduction to formate. *Angew. Chem. Int. Ed. Engl.* **2021**, *60*, 26233–26237.
38. Zheng, X.; De Luna, P.; García de Arquer, F.P.; et al. Sulfur-modulated tin sites enable highly selective electrochemical reduction of CO_2 to formate. *Joule* **2017**, *1*, 794–805.
39. Liang, C.; Kim, B.; Yang, S.; et al. High efficiency electrochemical reduction of CO_2 beyond the two-electron transfer pathway on grain boundary rich ultra-small SnO_2 nanoparticles. *J. Mater. Chem. A* **2018**, *6*, 10313–10319.
40. Luo, W.; Xie, W.; Li, M.; et al. 3D hierarchical porous indium catalyst for highly efficient electroreduction of CO_2. *J. Mater. Chem. A* **2019**, *7*, 4505–4515.
41. Gong, Q.; Ding, P.; Xu, M.; et al. Structural defects on converted bismuth oxide nanotubes enable highly active electrocatalysis of carbon dioxide reduction. *Nat. Commun.* **2019**, *10*, 2807.
42. Chen, C.; Shen, S.; Wang, J.; et al. Construction of a self-supporting bifunctional Sn–SnS_x electrocatalyst via one-step electrodeposition for formate production from coupled CO_2 reduction and glucose oxidation. *Green. Chem.* **2024**, *26*, 9888–9898.
43. He, S.; Ni, F.; Ji, Y.; et al. The p-orbital delocalization of main-group metals to boost CO_2 electroreduction. *Angew. Chem. Int. Ed.* **2018**, *57*, 16114–16119.
44. Wang, H.; Matios, E.; Wang, C.; et al. Rapid and scalable synthesis of cuprous halide-derived copper nano-architectures for selective electrochemical reduction of carbon dioxide. *Nano Lett.* **2019**, *19*, 3925–3932.
45. Li, M.; Song, N.; Luo, W.; et al. Engineering surface oxophilicity of copper for electrochemical CO_2 reduction to ethanol. *Adv. Sci.* **2023**, *10*, e2204579.
46. Wang, X.; Jiang, Z.; Wang, P.; et al. Ag^+-Doped InSe nanosheets for membrane electrode assembly electrolyzer toward large-current electroreduction of CO_2 to ethanol. *Angew. Chem.* **2023**, *135*, e202313646.
47. Gao, J.; Bahmanpour, A.; Kröcher, O.; et al. Electrochemical synthesis of propylene from carbon dioxide on copper nanocrystals. *Nat. Chem.* **2023**, *15*, 705–713.
48. Fuku, K.; Miyase, Y.; Miseki, Y.; et al. Enhanced oxidative hydrogen peroxide production on conducting glass anodes modified with metal oxides. *ChemistrySelect* **2016**, *1*, 5721–5726.
49. Liu, Y.; Zhao, S.-F.; Guo, S.-X.; et al. Electrooxidation of ethanol and methanol using the molecular catalyst [{$Ru_4O_4(OH)_2(H_2O)_4$}(γ-$SiW_{10}O_{36})_2$]$^{10-}$. *J. Am. Chem. Soc.* **2016**, *138*, 2617–2628.
50. Li, M.; Deng, X.; Xiang, K.; et al. Value-added formate production from selective methanol oxidation as anodic reaction to enhance electrochemical hydrogen cogeneration. *ChemSusChem* **2020**, *13*, 914–921.

51. Hao, Y.; Yu, D.; Zhu, S.; et al. Methanol upgrading coupled with hydrogen product at large current density promoted by strong interfacial interactions. *Energy Environ. Sci.* **2023**, *16*, 1100–1110.
52. Zhang, Y.; Han, Z.; Dong, B.; et al. A novel and effective strategy for electro-oxidation of ethanol to acetaldehyde. *Catal. Commun.* **2016**, *86*, 119–123.
53. Chen, G.-F.; Luo, Y.; Ding, L.-X.; et al. Low-voltage electrolytic hydrogen production derived from efficient water and ethanol oxidation on fluorine-modified FeOOH anode. *ACS Catal.* **2018**, *8*, 526–530.
54. Dai, L.; Qin, Q.; Zhao, X.; et al. Electrochemical partial reforming of ethanol into ethyl acetate using ultrathin Co_3O_4 nanosheets as a highly selective anode catalyst. *ACS Cent. Sci.* **2016**, *2*, 538–544.
55. Liu, Y.; Wang, L.; Zhang, Y.; et al. From ethylene glycol to glycolic acid: Electrocatalytic conversion on Pt-group metal surfaces. *Inorg. Chem.* **2024**, *63*, 14794–14803.
56. Matsumoto, T.; Sadakiyo, M.; Ooi, M.L.; et al. CO_2-free power generation on an iron group nanoalloy catalyst via selective oxidation of ethylene glycol in alkaline media. *Sci. Rep.* **2014**, *4*, 5620.
57. Yan, Y.; Fu, Y.; Yang, J.; et al. Electrocatalytic upcycling of polyethylene terephthalate waste to biodegradable polymer coupled with hydrogen production at ampere-level current density. *CCS Chem.* **2026**, *8*, 974–988.
58. Wu, T.; Zhu, X.; Wang, G.; et al. Vapor-phase hydrothermal growth of single crystalline NiS_2 nanostructure film on carbon fiber cloth for electrocatalytic oxidation of alcohols to ketones and simultaneous H_2 evolution. *Nano Res.* **2018**, *11*, 1004–1017.
59. Dai, C.; Sun, L.; Liao, H.; et al. Electrochemical production of lactic acid from glycerol oxidation catalyzed by AuPt nanoparticles. *J. Catal.* **2017**, *356*, 14–21.
60. Mahmoudian, J.; Bellini, M.; Pagliaro, M.V.; et al. Electrochemical coproduction of acrylate and hydrogen from 1,3-propandiol. *ACS Sustain. Chem. Eng.* **2017**, *5*, 6090–6098.
61. Chadderdon, D.J.; Xin, L.; Qi, J.; et al. Selective oxidation of 1,2-propanediol in alkaline anion-exchange membrane electrocatalytic flow reactors: Experimental and DFT investigations. *ACS Catal.* **2015**, *5*, 6926–6936.
62. Zheng, J.; Chen, X.; Zhong, X.; et al. Hierarchical porous NC@ CuCo nitride nanosheet networks: Highly efficient bifunctional electrocatalyst for overall water splitting and selective electrooxidation of benzyl alcohol. *Adv. Funct. Mater.* **2017**, *27*, 1704169.
63. You, B.; Liu, X.; Liu, X.; et al. Efficient H_2 evolution coupled with oxidative refining of alcohols via a hierarchically porous nickel bifunctional electrocatalyst. *Acs Catal.* **2017**, *7*, 4564–4570.
64. Jiang, N.; Liu, X.; Dong, J.; et al. Electrocatalysis of furfural oxidation coupled with H_2 evolution via nickel-based electrocatalysts in water. *ChemNanoMat* **2017**, *3*, 491–495.
65. Xia, H.; Xiang, D.; Liu, F.; et al. Boosting cathodic hydrogen evolution with furfuryl alcohol oxidation as the anodic half-reaction for hybrid water splitting. *Electrochim. Acta* **2023**, *441*, 141736.
66. Chen, D.; Yang, S.; Gao, J.; et al. Electrochemical co-upgrading CO_2 and glycerol for selective formate production with 190% overall Faradaic efficiency. *Nano Res.* **2025**, *18*, 94907399.
67. Li, X.; Gao, K.; Qu, M.; et al. Membrane-free CO_2 electrolyzer design for economically efficient formic acid electro-synthesis. *Nat. Commun.* **2025**, *16*, 9237.
68. Le, T.H.H.; Zuo, Y.; Chatti, M.; et al. Coupling of CuO@ $NiBiO_x$ catalyzed glycerol oxidation to carbon dioxide reduction reaction for enhanced energy efficiency. *Angew. Chem.* **2025**, *64*, e202502617.
69. Lu, C.; Yang, S.; Shi, P.; et al. Integrated electrochemical biomass oxidation and CO_2 reduction over ultra-wide potential window. *Angew. Chem.* **2025**, *137*, e202502846.
70. Liu, S.-Q.; Gao, M.-R.; Wu, S.; et al. A coupled electrocatalytic system with reduced energy input for CO_2 reduction and biomass valorization. *Energy Environ. Sci.* **2023**, *16*, 5305–5314.
71. Zhang, Z.; Liu, S.; Wu, Z.; et al. High efficiency coupled electrocatalytic CO_2 reduction to C_2H_4 with 5-hydroxymethylfurfural oxidation over Cu-based nanoflower electrocatalysts. *Green. Chem.* **2023**, *25*, 5404–5415.
72. Zhou, Y.; Wang, Z.; Fang, W.; et al. Modulating O–H activation of methanol oxidation on nickel-organic frameworks for overall CO_2 electrolysis. *ACS Catal.* **2023**, *13*, 2039–2046.
73. Kang, C.; Li, Y.; Xu, Y.; et al. Coupling CO_2-to-ethylene reduction with the chlor-alkaline process in seawater through in situ-formed Cu catalysts. *J. Phys. Chem. Lett.* **2023**, *14*, 2983–2989.
74. Yu, X.; Rabiee, H.; Dutta, A.; et al. Upcycling CO_2 and PET waste: Ampere-level formate electrosynthesis in an integrated electrolyzer. *J. Am. Chem. Soc.* **2025**, *147*, 41481–41491.
75. Pei, Y.; Pi, Z.; Zhong, H.; et al. Glycerol oxidation-assisted electrochemical CO_2 reduction for the dual production of formate. *J. Mater. Chem. A* **2022**, *10*, 1309–1319.
76. Wang, X.; Li, P.; Tam, J.; et al. Efficient CO and acrolein coproduction via paired electrolysis. *ECS Meet. Abstr.* **2024**, *7*, 931–937.
77. Zhang, M.; Liao, J.-P.; Li, R.-H.; et al. Green synthesis of bifunctional phthalocyanine-porphyrin COFs in water for efficient electrocatalytic CO_2 reduction coupled with methanol oxidation. *Natl. Sci. Rev.* **2023**, *10*, nwad226.

78. Vehrenberg, J.; Baessler, J.; Decker, A.; et al. Paired electrochemical synthesis of formate via oxidation of glycerol and reduction of CO_2 in a flow cell reactor. *Electrochem. Commun.* **2023**, *151*, 107497.
79. Segets, D.; Andronescu, C.; Apfel, U.-P. Accelerating CO_2 electrochemical conversion towards industrial implementation. *Nat. Commun.* **2023**, *14*, 7950.
80. Ozden, A.; Li, J.; Kandambeth, S.; et al. Energy-and carbon-efficient CO_2/CO electrolysis to multicarbon products via asymmetric ion migration–adsorption. *Nat. Energy* **2023**, *8*, 179–190.
81. Siegmund, D.; Metz, S.; Peinecke, V.; et al. Crossing the valley of death: From fundamental to applied research in electrolysis. *Jacs Au* **2021**, *1*, 527–535.
82. Ko, B.H.; Hasa, B.; Shin, H.; et al. The impact of nitrogen oxides on electrochemical carbon dioxide reduction. *Nat. Commun.* **2020**, *11*, 5856.
83. Xu, Y.; Edwards, J.P.; Zhong, J.; et al. Oxygen-tolerant electroproduction of C_2 products from simulated flue gas. *Energy Environ. Sci.* **2020**, *13*, 554–561.
84. Lu, C.-H.; Chen, T.-L.; Chen, K.-W.; et al. From electrons to formic acid: rigorous process synthesis and sustainability assessment of a fully integrated electrochemical CO_2 valorization system. *ACS Sustain. Chem. Eng.* **2026**, *14*, 13457–13471.
85. Li, Y.C.; Yan, Z.; Hitt, J.; et al. Bipolar membranes inhibit product crossover in CO_2 electrolysis cells. *Adv. Sustain. Syst.* **2018**, *2*, 1700187.
86. Wang, Z.; Yan, J.; Wang, H.; et al. Separation and conversion of CO_2 reduction products into high-concentration formic acid using bipolar membrane electrodialysis. *J. Membr. Sci.* **2024**, *708*, 123016.
87. Chien, I.L.; Yu, B.-Y.; Ai, Z.J. Chapter 15—Design of Azeotropic Distillation Systems. In *Chemical Engineering Process Simulation*; Elsevier: Amsterdam, The Netherlands, 2017; pp. 355–385.
88. Yu, B.-Y.; Huang, R.; Zhong, X.-Y.; et al. Energy-efficient extraction–distillation process for separating diluted acetonitrile–water mixture: Rigorous design with experimental verification from ternary liquid–liquid equilibrium Data. *Ind. Eng. Chem. Res.* **2017**, *56*, 15112–15121.
89. Yu, B.-Y.; Chien, I.L. Novel temperature-control strategy for single column side-stream extractive distillation process with intermediate-boiling entrainer. *Sep. Purif. Technol.* **2023**, *310*, 123163.
90. Hori, Y.; Kikuchi, K.; Suzuki, S. Production of CO and CH_4 in electrochemical reduction of CO_2 at metal electrodes in aqueous hydrogencarbonate solution. *Chem. Lett.* **1985**, *14*, 1695–1698.
91. Royer, M. Réduction de l'acide carbonique en acide formique. *Compt. Rend.* **1870**, *1870*, 731–732.
92. Bevilacqua, M.; Filippi, J.; Lavacchi, A.; et al. Energy savings in the conversion of CO_2 to fuels using an electrolytic device. *Energy Technol.* **2014**, *2*, 522–525.
93. Li, T.; Cao, Y.; He, J.; et al. Electrolytic CO_2 reduction in tandem with oxidative organic chemistry. *ACS Cent. Sci.* **2017**, *3*, 778–783.
94. Wang, G.; Chen, J.; Li, K.; et al. Cost-effective and durable electrocatalysts for Co-electrolysis of CO_2 conversion and glycerol upgrading. *Nano Energy* **2022**, *92*, 106751.
95. Xie, K.; Ozden, A.; Miao, R.K.; et al. Eliminating the need for anodic gas separation in CO_2 electroreduction systems via liquid-to-liquid anodic upgrading. *Nat. Commun.* **2022**, *13*, 3070.
96. Liu, S.; Tian, B.; Xu, X.; et al. Ampere-level electrolytic coproduction of formate with coupled carbon dioxide reduction and selective methanol oxidation. *ACS Catal.* **2024**, *14*, 9476–9486.
97. Lin, J.; Chi, H.; Liu, H.; et al. Concentrated formate produced through co-electrolysis of CO_2 and methanol in a zero-gap electrolyzer. *AIChE J.* **2024**, *70*, e18382.
98. Zhang, H.; Bo, Z.; Wang, M.; et al. Copper-stabilized bismuth subcarbonate electrocatalysts for durable large-scale formate production at kilowatt power. *Nat. Commun.* **2025**, *17*, 577.